Received: 20 February 2021 | Revised: 24 May 2021 | Accepted: 9 June 2021

DOI: 10.1111/ijag.16322

INTERNATIONAL JOURNAL OF Applied Glass SCIENCE

SPECIAL ISSUE ARTICLE

Structural and optical properties in Tm^{3+}/Tm^{3+}–Yb^{3+} doped $NaLuF_4$ glass-ceramics

Jose J. Velázquez[1] | **Rolindes Balda**[2,3] | **Joaquin Fernández**[4] | **Giulio Gorni**[5,6] | **Mercedes Sedano**[5] | **Alicia Durán**[5] | **Dušan Galusek**[1,7] | **Maria J. Pascual**[5]

[1]FunGlass, Alexander Dubček University of Trenčín, Trenčín, Slovakia

[2]Applied Physic Department I, Superior School of Engineering, Basque Country University, Bilbao, Spain

[3]Materials Physics Center, CSIC-UPV/EHU, San Sebastian, Spain

[4]Donostia International Physics Center, San Sebastian, Spain

[5]Ceramic and Glass Institute (ICV-CSIC), Madrid, Spain

[6]Cells, ALBA Synchrotron, Cerdanyola del Vallès, Spain

[7]Joint Glass Centre of the IIC SAS, TnUAD, and FChPT STU, Trenčín, Slovakia

Correspondence
Jose J. Velázquez, FunGlass, Alexander Dubček University of Trenčín, Študentská 2, 911 50 Trenčín, Slovakia.
Email: jose.velazquez@tnuni.sk

Funding information
Euskal Herriko Unibertsitatea, Grant/Award Number: GIU17/014; European Regional Development Fund, Grant/Award Number: 313011R453 and 313011W442; Ministerio de Economía y Competitividad, Grant/Award Number: MAT2017-87035-C2-1-P/-2-P; the European Union´s Horizon 2020 research and innovation programme, Grant/Award Number: 739566; Gobierno del Pais Vasco, Eusko Jaurlaritza, Grant/Award Number: PIBA2018-24

Abstract

Transparent $NaLuF_4$ glass-ceramics (GCs) doped with Tm^{3+} and Tm^{3+}/Yb^{3+} have been prepared by melting-quenching followed by thermal treatment at temperatures near the glass transition temperature. The crystallization process has been studied using X-ray diffraction (XRD) and high-resolution transmission electron microscopy (HRTEM). $NaLuF_4$ nanocrystals (NCs) ranging 9–30 nm in size are the only crystalline phase, the crystal size increasing with the dopant concentration. Energy dispersive X-ray (EDX) measurements confirm the Tm^{3+} and Yb^{3+} incorporation in the NCs. Optical characterization included the analysis of up-conversion (UC) as well as the Near-infrared (NIR) luminescence. NIR emission spectra of Tm^{3+} and Yb^{3+} in co-doped samples confirmed an efficient energy transfer between both ions. No UC emissions are observed in Tm^{3+} single-doped glass and GCs. Yb^{3+} incorporation favors the Tm^{3+}-Tm^{3+} UC processes resulting in Tm^{3+} blue, yellowish-red and NIR UC emissions after excitation at 975 nm. Blue UC emission is also observed in the codoped samples after Tm^{3+} excitation at 791 nm. These effects were more evident for the GCs compared to the base glasses, confirming the RE ions incorporation in the NCs. As a result, these GCs can be used to tune the UC emission from NIR to blue by selective excitation.

KEYWORDS

crystallization, glass ceramics, glass manufacturing, optical properties, photo luminescence, processing, secondary

1 | INTRODUCTION

The search for new and more developed luminescent systems is still a challenge due to the wide range of optical applications that requires higher efficiencies, such as plasma display panels; white light-emitting diodes; fluorescent lamps, optical biosensors or biological markers, and laser cooling of solids.[1–6] Between these systems, rare-earth (RE)-doped nanostructured oxyfluoride glass-ceramics (OxGCs) are very interesting materials due to the combination of the low phonon-energy (300-400cm^{-1}) fluoride nanocrystals (NCs), with the mechanical, thermal, and chemical properties of oxide glasses.[7,8] Moreover, the controlled crystallization mechanism allows obtaining NCs with sizes up to 50 nm in which the RE ions are incorporated, dismissing the Rayleigh scattering and maintaining the transparency.[9]

Glass-ceramics based on LaF_3, YF_3, and $RLnF_4$ (R = K, Na)[10–13] phases have been described as efficient luminescent materials. In particular, sodium lanthanide tetrafluorides, with the general formula $NaLnF_4$, (with Ln = Gd, Y, La, or Lu) have been reported to be ideal hosts for RE^{3+} ions that can act as emitting centers and have been widely studied.[14–17]

$NaLuF_4$ exhibits two possible crystalline phases, cubic (α) and hexagonal (β), and it is an exceptional converter host for RE^{3+} ions.[18,19] Nevertheless, the number of publications regarding $NaLuF_4$ GCs obtained by melting-quenching is relatively scarce mainly due to the difficulty to obtain the desired crystalline phase with the proper degree of crystallization.[20,21] GCs from the base composition $70SiO_2$–$8.5B_2O_3$–$9.5Na_2CO_3$–6NaF-$6LuF_3$ (mol%) were developed by Chen et al.[22] In this work, visible UC luminescence was obtained after excitation at 980 nm of Yb^{3+} ions and subsequent energy transfer to Er^{3+} or Tm^{3+}. The UC luminescence intensity of the GCs increase around 10000 and 2000 times, respectively, compared to the corresponding glass. Kück et al.[23] described the optical properties of the Pr^{3+}-doped pure $Na_7Lu_{13}F_{46}$ crystalline phase and concluded that that system is suitable for use in cascade-emitting phosphors for Xe discharge lamps.

From the different RE ions, Tm^{3+} ions exhibit interesting characteristics that in conjunction with the Yb^{3+} ions make them suitable candidates for laser operation at 0.8 and 1.5 μm.[24–26] The Tm^{3+} ions have three metastable excited levels, $^1D_2$, $^1G_4$, and $^3H_4$ that allows the emission in the blue, red, and infrared regions after pumping. Another characteristic is that the emission from the $^3H_4$ level to the ground state coincides with the window of the silica fibers near 0.8 μm. Moreover, many different energy transfer channels are possible between Yb^{3+} – Tm^{3+} due to the existence of significant resonance energy levels.[27]

In our previous works,[28–30] sodium lutetium fluoride glass-ceramics doped with ErF_3 and codoped with ErF_3-YbF_3 were studied in detail from a structural and optical perspective and for their suitable use in optical fibers. Transparent GCs based on a cubic solid solution $Na_xLu_{2x-1}F_{7x-3}$ were successfully synthesized and the incorporation of RE^{3+} ions was confirmed by XRD and energy dispersive X-ray spectroscopy (EDX).[28] In the present work, the crystallization mechanism, and structural and optical properties of Tm^{3+}-doped and Tm^{3+}–Yb^{3+} co-doped GCs are reported from the same base glass composition, $70SiO_2$–$5Al_2O_3$–$2AlF_3$–$2Na_2O$–18NaF–$3Lu_2O_3$ (mol%). Particular attention is paid to the effect of co-doping and RE^{3+}-ion concentration on the crystallization kinetics and UC and NIR emissions.

2 | EXPERIMENTAL PROCEDURE

Glasses with the composition $70SiO_2$–$5Al_2O_3$–$2AlF_3$–$2Na_2O$–18NaF–$3Lu_2O_3$ (mol%) doped with xTmF$_3$, x = 0.1, 0.5 and codoped with yYbF$_3$, y = 0, 1, and 2 (mol%) have been prepared by the melting-quenching method. This composition was based on a previous study of the research group.[30] The raw materials on reagent grade were SiO_2 sand (Saint-Gobain, 99.6%), Al_2O_3 (Panreac), Na_2CO_3 (Panreac, 99.5%), NaF (Panreac, 99.95%), Lu_2O_3 (Alfa Aesar, 99.9%), AlF_3 (Alfa Aesar, 99.9%), TmF_3 (Aldrich, 99.99%), and YbF_3 (Alfa Aesar, 99.999%). The raw materials were mixed in a Turbula mixer for 3 h. The batches of 100 g. were calcined at 1250°C for 0.5 h and melted at 1650°C for 1 h in a Pt crucible with 125 cm^3 in volume covered with a Pt cap and then quenched on a brass mold. The melting process was repeated twice to improve the glass homogeneity. The glasses were annealed at 580°C for 30 min to remove residual stresses. From now on, the obtained glass samples will be labelled as G0.1Tm, G0.5Tm, G0.5Tm-1Yb, and G0.5Tm-2Yb, for 0.1, 0.5 Tm^{3+} and 1, and 2 Yb^{3+} concentrations (in mol%), respectively; corresponding glass-ceramics will be denoted as GC. Glass specimens were heat-treated at 600°C for 20 h, using a heating rate of 10°C/min to get the corresponding GCs. To perform the optical characterization, polished glass sheets (1cm x 1cm and thickness of 2 mm) heat-treated at 600°C during 20 h were selected. One polished sheet of base glass of each composition and with the same shape was also used for comparison with the corresponding glass-ceramics.

The thermal properties of the obtained glasses (glass transition temperature (T_g), softening point (T_d), and thermal expansion coefficient (α)) were determined by

dilatometry. The dilatometric analysis was carried out using a Netzsch Gerätebau dilatometer, model 402 PC/1 with a heating rate of 5°C /min in the air; the estimated error of T_g is ±2°C. The thermal expansion coefficient was determined in the range 100°C–450°C.

The chemical composition of the glass samples, focussing on the Fluorine content, was analyzed by X-ray fluorescence spectroscopy (XRF) using a PANalytical spectrometer. All oxides were determined employing the melting method with $Li_2B_4O_7$, whereas elemental fluorine analysis was performed on pressed pellets of powdered glass (63 μm, 0.3 g) in order to avoid fluorine volatilization.

Sieved glass-ceramic powders with the particle size <63 μm were used for both XRD and TEM analysis. XRD measurements have been performed with an X-ray diffractometer D8 ADVANCE (Bruker) equipped with a Lynx Eye detector. The patterns were collected with monochromatic Cu$K_{\alpha 1}$ radiation (λ = 1.54056 Å). Diffractograms were collected in the range in the $10 \leq 2\theta \leq 70°$ using a step size of 0.02 ° and 1 s. the acquisition time for each step. This technique was used to achieve two objectives; determination of the crystalline phase and estimation of the crystal size. For crystalline phases determination, the EVADiffractPLUS software was used meanwhile mean crystal sizes were resolved from the Scherrer equation with the corresponding errors.[31]

$$\varnothing = \frac{0.94 \cdot \lambda}{\cos\theta\sqrt{\beta^2 - \beta_i^2}}, \quad (1)$$

where θ is the angle of the diffraction maximum, β its full width at half maximum (FWHM), β_i the instrumental broadening and λ is the wavelength. The θ and β parameters were obtained by fitting the most intense peaks to pseudo-Voigt functions.

High-resolution transmission electron microscopy (HR-TEM), including scanning transmission microscopy-high angle annular dark field (STEM-HAADF) and X-ray energy dispersive spectroscopy (EDXS), were recorded on a JEOL 2100 field emission gun transmission electron microscope operating at 200 kV and providing a point resolution of 0.19 nm. The TEM was equipped with an EDXS energy dispersive X-ray spectrometer (INCA x-sight, Oxford Instruments). EDX analysis was performed in STEM mode, with a probe size of ca. 1 nm. Samples were prepared by dispersing the fine powder in ethanol with ultrasonic agitation; a droplet of the suspension was put on a copper holey carbon grid.

Conventional transmission spectra were performed with a Cary 5 spectrophotometer. The steady-state emission measurements were made with a Ti-sapphire ring laser (0.4 cm^{-1} linewidth) as exciting light. The fluorescence was analyzed with a 0.25 monochromator, and the signal was detected by an extended IR Hamamatsu H10330A-75 photomultiplier and finally amplified by a standard lock-in technique. Visible emission was detected by a Hamamatsu R636 photomultiplier. All measurements were performed at room temperature. Accuracy of emission measurements is between 3% and 5% depending on the experimental conditions.

3 | RESULTS AND DISCUSSION

3.1 | Thermal, XRD, and HRTEM analysis

Transparent glasses were obtained after melting for the different dopant concentrations. As expected, the corresponding XRD patterns (not shown) did not reveal the presence of any crystalline phase. Thermal properties were characterized by dilatometric analysis and results are shown in Table 1. T_g does not show any constant increasing tendency with the dopant content, but the doped and codoped samples present T_g values ranging from 566°C to 589°C.

At the same time, the thermal expansion coefficient (α) has the same value as in the undoped glass, 7.9°C^{-1}, decreasing for the codoped glasses down to 7.3°C^{-1} with the increasing amount of Yb^{3+} ions. Similar behaviour was found by the authors for the same composition but

TABLE 1 Fluorine loss (%), Glass transition temperature (T_g), softening point temperature (T_d) and thermal expansion coefficient (α) of undoped and doped glasses. Mean NCs size and thermal expansion coefficient (α) of corresponding GCs

Glass	F loss (%)	$\alpha\ 10^{-6}$ (°C^{-1}) ±0.5	T_g (°C) ±2	T_d (°C) ±5	GCs	NCs size (nm) ±1	$\alpha\ 10^{-6}$ (°C^{-1}) ±0.5
Undoped	48	7.9	579	663	Undoped	9	8.6
G0.1Tm	42	7.9	583	664	GC0.1Tm	12	8.2
G0.5Tm	45	7.9	566	648	GC0.5Tm	15	8.6
G0.5Tm−1Yb	42	7.6	589	685	GC0.5Tm−1Yb	27	7.9
G0.5Tm−2Yb	52	7.3	572	673	GC0.5Tm−2Yb	30	9.0

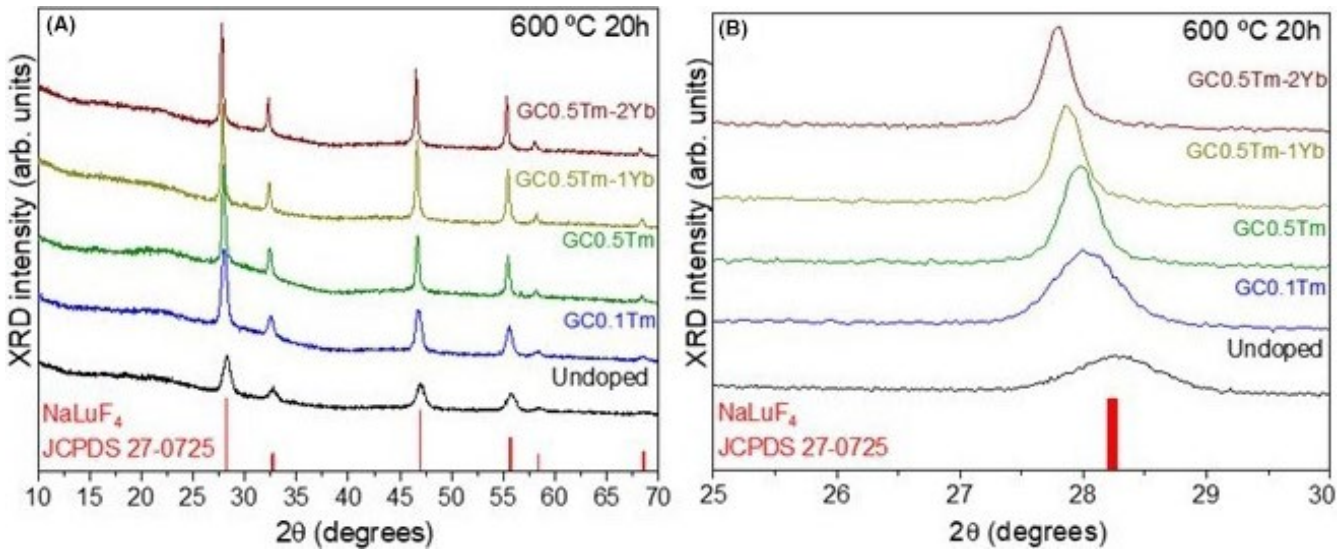

FIGURE 1 (A) XRD patterns for undoped, $x\mathrm{Tm}^{3+}$-doped (x = 0.1, 0.5 mol%) and $0.5\mathrm{Tm}^{3+}$–$y\mathrm{Yb}^{3+}$-codoped (y = 1, 2 mol%) GCs. (B) Magnified regions of (111) peak of the corresponding GCs

doped and codoped with Er^{3+} and Yb^{3+} ions.[28] Moreover, Sroda, Gorni and de Pablos-Martin et al. also observed a similar effect in different oxyfluoride glasses.[16,32,33] The thermal expansion coefficient of GCs samples was also measured and the values are shown in Table 1. In general, all GCs show higher values than the glass samples but in the range of error. This behavior is opposite to that observed by Reben and Środa in PbF_2 NCs glass, where the addition of fluorine decreased the thermal expansion coefficient and weakened the structure of the glass.[34] In our case, it seems that the amount of fluorine incorporation in the structure due to the addition of dopant is not sufficient to affect the structure of the glassy phase in the GCs.

Table 1 also presents the estimated F loss of each glass obtained from the chemical analysis of the corresponding glasses. From these results, the fluorine loss varies between 42 and 52 wt%. The chemical analysis of the other components (not shown) displays values roughly in agreement with the nominal ones. These values indicate that a high fluorine loss occurs during the melting process due to the high melting temperatures involved, at around 1650°C, as is expected in these compositions.

Taking into account the effect of the dopant addition on the glass T_g and our previous results,[28–30,35] the heat treatment temperature and time were selected as 600°C during 20 h. Figure 1A shows the XRD patterns of the corresponding GCs samples. The results for the different dopant concentrations are almost identical with the diffraction maxima that are assigned to sodium lutetium fluoride cubic solid solution with a general formula $Na_xLu_{2x-1}F_{7x-3}$ as previously reported in.[28,30] The peaks become narrower and more intense when increasing dopant content indicating that the NCs growth is favoured. Moreover, the magnified region correspondings to the (111) crystallographic plane, Figure 1B, shows a constant shift towards lower angles with the increasing content of RE^{3+} dopant ions, mainly due to incorporation of the larger Tm^{3+} (ionic radius, r_{ion} = 0.88 Å) and Yb^{3+} ions (r_{ion} = 0.87 Å) that substitute the Lu^{3+} (r_{ion} = 0.85 Å) increasing the unit cell volume associated to the cubic phase.

Table 1 also shows the mean size of NCs calculated by using the Scherrer equation. The increasing dopant content results in increasing size, varying from 9 to 30 nm. In this case, the dopant content plays a notable role in crystal growth as observed for other GCs.[36,37] The increasing NCs size is also related to the close relationship between the crystallization activation energy and doping level. Crystallization activation energy decreases with the increasing doping level.[38] Thus, samples with higher dopant concentration are more susceptible to crystallize.

HRTEM together with EDX techniques were used to look deeply into the nanostructure and dopants distribution, see Figures 2 and 3. HRTEM micrographs of the glasses, Figure 2A,B, show the typical well-dispersed phase-separated amorphous droplets. These phase-separated droplets are the precursors of the $NaLuF_4$ NCs that will form after adequate heat treatment[28] observed in Figure 2C,D. Moreover, HRTEM micrographs of GC0.5Tm–2Yb show a broad crystal distribution that fits well with a pseudo-Voight function centered at 13 nm (inset Figure 2C), confirming the results obtained by XRD diffraction. It should be noted that unlike the hexagonal LaF_3 oxyfluoride NCs,[33,39] cubic $NaLuF_4$ NCs form from each phase-separated droplet, this is typical behavior of alkali lanthanide tetrafluoride NCs.[13,40,41] The size of the NCs is thus similar to the size of the precursor phase-separated

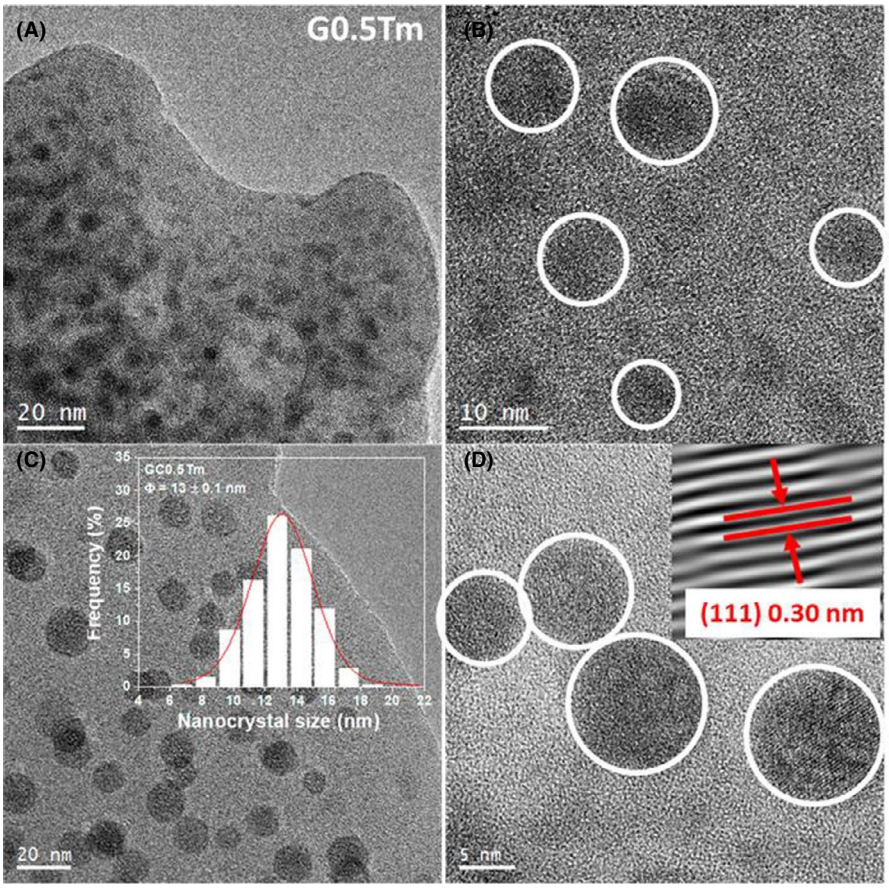

FIGURE 2 (A) and (C) HRTEM micrograph of 0.5Tm^{3+} doped glass and GC treated at 600°C-20 h; size distribution of the NCs is shown as insets in (C). (B) Magnified image of phase separation droplets. (D) HRTEM micrograph of 0.5Tm^{3+}-doped GCs with corresponding SAED image shown as an inset

regions, and then they grow more with the adequate heat treatment in temperature and time.[28] Moreover, the Fast Fourier Transformation (FFT) from HRTEM micrographs revealed crystalline structures with interplanar distances of 0.31 nm, attributed to (111) planes of the sodium lutetium fluoride cubic phase.

To further study, the elemental composition and the incorporation of the RE^{3+} ions in the NCs, EDX analysis in STEM mode was performed for the Tm^{3+}-doped and Tm^{3+}-Yb^{3+} codoped GCs (Figure 3). This indicates the nanocrystals are Na- and Lu-rich, with the Tm^{3+} and Yb^{3+} ions concentrated in the nanocrystals, similarly to previously observed for different fluoride NCs and RE^{3+} dopants.[14,16,42] The presence of the Tm^{3+} and Yb^{3+} ions in the NCs supports the results obtained by XRD patterns in which the diffraction maxima are shifted to lower angles, suggesting the incorporation of the RE^{3+} ions in the crystal structure of the NCs.

3.2 | Optical properties

3.2.1 | Transmission spectra

The transmission spectra were obtained for all samples in the 300–2000 nm range. As an example, Figure 4 shows the spectra as a function of wavelength for the glass and GC samples codoped with 0.5TmF_3-1YbF_3 (in mol%). The spectra show the bands corresponding to the transitions starting from the $^3H_6$ ground state to the different higher levels $^1D_2$, $^1G_4$, $^3F_2$, $^3F_3$, $^3H_4$, $^3H_5$, and $^3F_4$ of Tm^{3+} together with the $^2F_{7/2} \rightarrow {}^2F_{5/2}$ absorption of Yb^{3+}. As can be seen, the samples are transparent with a transmittance as high as 91% and 89% for the glass and glass-ceramic, respectively. After the heat treatment, the absorption edge is shifted to longer wavelengths in the GC sample. This red-shift has been attributed to the scattering of short-wavelength light by the NCs present in the GC sample.[43,44] The spectra obtained for the glass and glass-ceramic samples doped with 2 mol% YbF_3 are similar, except for the double Yb^{3+} band intensity.

3.2.2 | NIR luminescence

The near-infrared emission in the 900–2200 nm spectral range was obtained for the single doped samples at room temperature by exciting at 791 nm in resonance with the $^3H_4$ (Tm^{3+}) level. The codoped samples were also excited at 975 nm in resonance with the $^2F_{7/2} \rightarrow {}^2F_{5/2}$ absorption of Yb^{3+}. This wavelength corresponds to the maximum absorption of Yb^{3+} ions in these matrices. The fluorescence

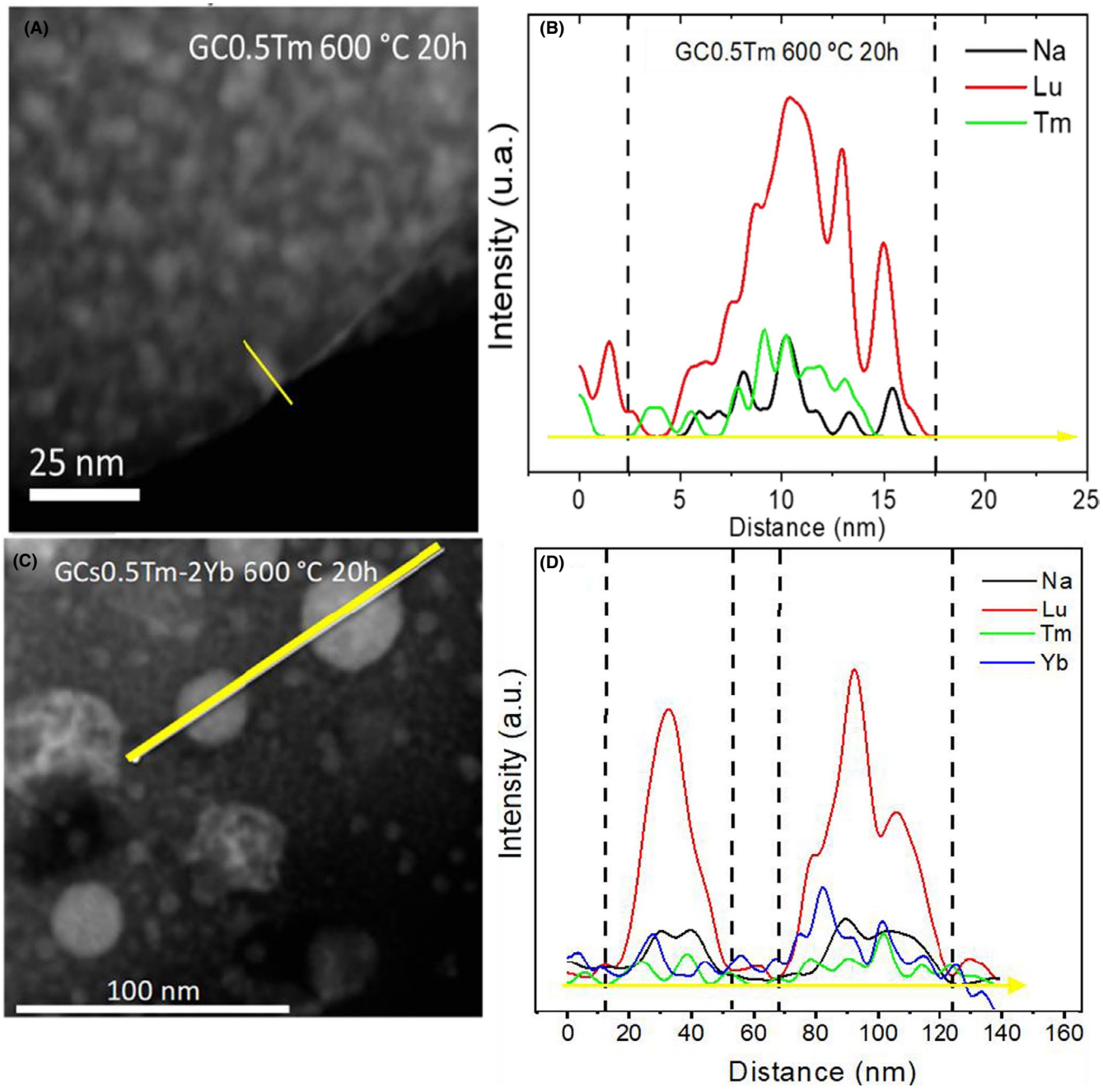

FIGURE 3 (A) and (C) STEM image of $NaLuF_4$ NCs in $GC0.5Tm^{3+}$ and $GC0.5Tm^{3+}$–$2Yb^{3+}$. (B) and (D) EDX of a line scan crossing same $aLuF_4$ NCs in $GC0.5Tm^{3+}$ and $GC0.5Tm^{3+}$–$2Yb^{3+}$

spectra corresponding to the single doped samples doped with 0.1 and $0.5Tm^{3+}$ (in mol%) are shown in Figure 5. The spectra show a strong emission band centered around 1650 nm which corresponds to the $^3F_4 \rightarrow {}^3H_6$ transition together with a less intense emission band centered around 1450 nm and corresponding to the $^3H_4 \rightarrow {}^3F_4$ transition. The long-wavelength tail of the $^3F_4 \rightarrow {}^3H_6$ emission is not completely observed due to the upper limit of the detector. Similar spectra are obtained for the glass and glass-ceramic samples, but the ratio of the emission intensity of the transition $^3H_4 \rightarrow {}^3F_4$ to that of the $^3F_4 \rightarrow {}^3H_6$ decreases with increasing Tm^{3+} concentration as is shown in Figure 5. This reduction in the intensity of the 1450 nm emission with concentration has been attributed to cross-relaxation between $^3H_4 \rightarrow {}^3F_4$ and $^3F_4 \rightarrow {}^3H_6$ transitions that enhance the latter.[45,46]

The emission spectra of the codoped samples obtained under the same experimental conditions by exciting at 791 nm show, in addition to the Tm^{3+} emissions around 1450 and 1650 nm, the Yb^{3+} ($^2F_{5/2} \rightarrow {}^2F_{7/2}$) emission around 1000 nm. The presence of the Yb^{3+} emission after excitation of Tm^{3+} ions confirms the energy transfer from

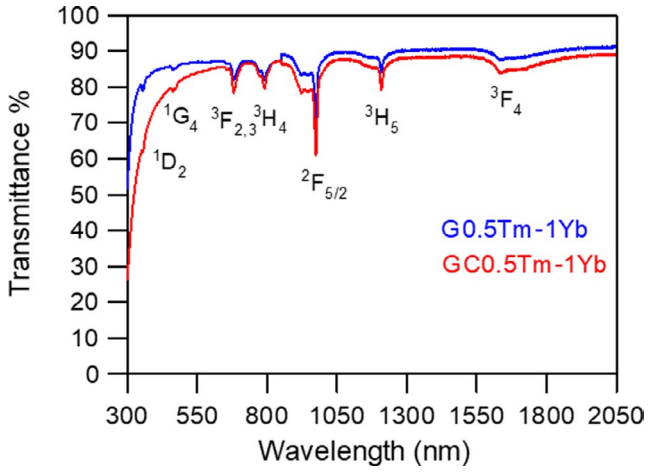

FIGURE 4 Transmission spectra for glass and glass-ceramic (GC) samples codoped with 0.5 mol% $Tm^{3+}$and 1 mol% Yb^{3+}

Tm^{3+} to Yb^{3+} ions. As an example, Figure 6 displays the emission spectra for the codoped samples with 0.5Tm-1Yb. After excitation of level $^3H_4$, the energy transfer to the $^2F_{5/2}$ state of Yb^{3+} ions occurs. Although the $^3H_4$ and $^3H_5$ levels of Tm^{3+} are located at higher and lower energies respectively, a non-resonant phonon-assisted energy transfer (PAET) between both ions takes place.[47,48]

The NIR luminescence intensities of the Tm^{3+} emissions measured under 791 nm (Tm^{3+}) excitation, in the single and codoped samples with 1 mol% of Yb^{3+} (Figures 5B and 6) are quite similar for the $^3F_4 \rightarrow {}^3H_6$ transition and nearly independent of the presence of Yb^{3+}. However, the intensity of the $^3H_4 \rightarrow {}^3F_4$ transition slightly decreases with the addition of Yb^{3+} ions probably due to the $Tm^{3+} \rightarrow Yb^{3+}$ energy transfer. Once the $^3H_4$ level is populated by the absorption of 791 nm photons, energy is transferred to the $^2F_5$ state of Yb^{3+}.

Moreover, the presence of energy transfer from Yb^{3+} to Tm^{3+} is demonstrated by the observation of the $^3F_4 \rightarrow {}^3H_6$ Tm^{3+} emission after excitation at 975 nm in resonance with the Yb^{3+} absorption at 975 nm, as shown in Figure 7. This figure shows the spectra of the glass and glass-ceramic samples codoped with 1 and 2 mol% of Yb^{3+}. As can be seen, the emission intensity for the co-doped samples with 2 mol% of Yb^{3+} is around twice those of the samples with 1 mol%. Moreover, compared to the emission obtained under Tm^{3+} excitation at 791 nm, the intensity of the $^3F_4 \rightarrow {}^3H_6$ increases around four times when exciting Yb^{3+} ions. This is in agreement with the high absorption cross-section of Yb^{3+} at 975 nm if compared with the one of Tm^{3+} at 791 nm. The $^2F_{5/2}$ (Yb^{3+})→$^3H_5$(Tm^{3+}) energy transfer followed by nonradiative processes populate the $^3F_4$ emitting level.

3.2.3 | NIR to visible up-conversion (UC)

Up-conversion (UC) emission from Tm^{3+} ions in the co-doped samples has been observed at room temperature after 975 nm excitation. The UC emission spectra show bands at 478, 651, 700, and 800 nm corresponding to the $^1G_4 \rightarrow {}^3H_6$, $^1G_4 \rightarrow {}^3F_4$, $^3F_{2,3} \rightarrow {}^3H_6$, and $^3H_4 \rightarrow {}^3H_6$ transitions of Tm^{3+} ions respectively.

Figure 8 shows that the increase in the UC intensity in the GCs with respect to those obtained in the glass. However, this increment is not as big as expected. Thus, the small increase in the UC emission intensity in the GCs, if compared with the untreated glass deserves a particular comment. It looks like that after the heat treatment the fraction of RE^{3+} ions in the amorphous and crystalline phases could change if compare with those of the precursor glass. In particular, the presence of Yb^{3+} ions

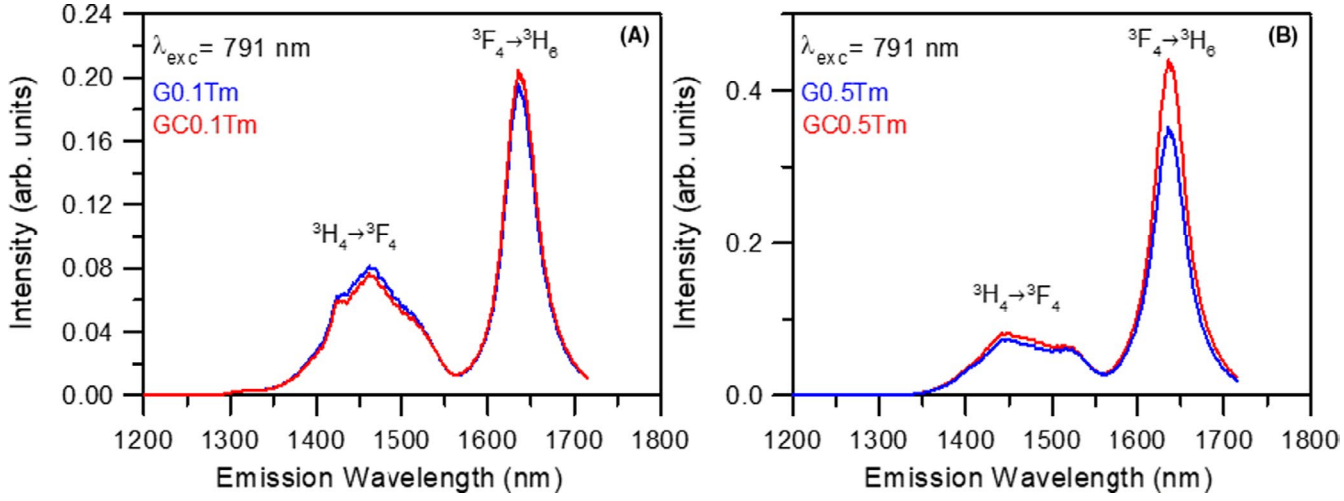

FIGURE 5 Room temperature emission spectra of Tm^{3+} ions in the single doped glass and GC samples doped with (A) 0.1 and (B) 0.5 mol% Tm^{3+}

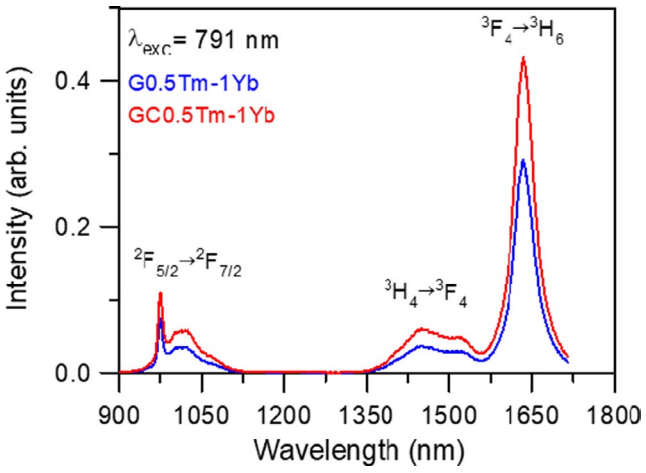

FIGURE 6 Room temperature emission spectra of Tm^{3+} and Yb^{3+} ions in the codoped glass and GC samples codoped with $0.5Tm^{3+}$-$1Yb^{3+}$ obtained under excitation at 791 nm

competing with Tm^{3+} ions in a finite crystalline volume would reduce the density of the UC centers and, therefore, the UC efficiency.

Moreover, increasing the Yb^{3+} content up to 2 mol% does not lead to an increase in the total Tm^{3+} UC luminescence. Moreover, the overall intensity is lower. This effect could be attributed to energy migration among Yb^{3+} ions due to the higher concentration, to energy back transfer from Tm^{3+} to Yb^{3+} and/or to energy transfer to quencher centers.[49]

The UC processes involved in the population of the relevant emitting states of Tm^{3+} ion are depicted in Figure 9. Firstly, the Yb^{3+} ion at the ground state was excited to the $^2F_{5/2}$ state by absorbing one 975 nm photon and then transferred the energy to Tm^{3+} ions in the ground state following the mechanism $^2F_{5/2} \rightarrow {}^2F_{7/2}$ (Yb^{3+}):$^3H_6 \rightarrow {}^3H_5$ (Tm^{3+}) (ET1). The $^3H_5$ level decays mainly non-radiatively populating the $^3F_4$ (Tm^{3+}) state. Then, a second energy

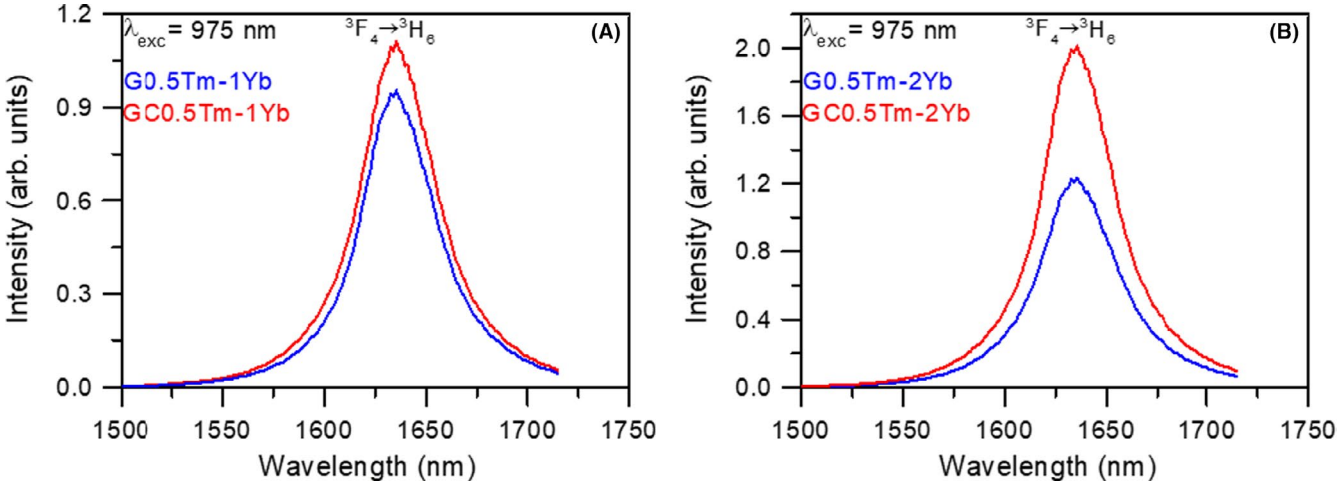

FIGURE 7 Room temperature emission spectra of Tm^{3+} ions in the glass and GC samples codoped with (A) $0.5Tm^{3+}$-$1Yb^{3+}$ and (B) $0.5Tm^{3+}$-$2Yb^{3+}$ obtained under excitation at 975 nm

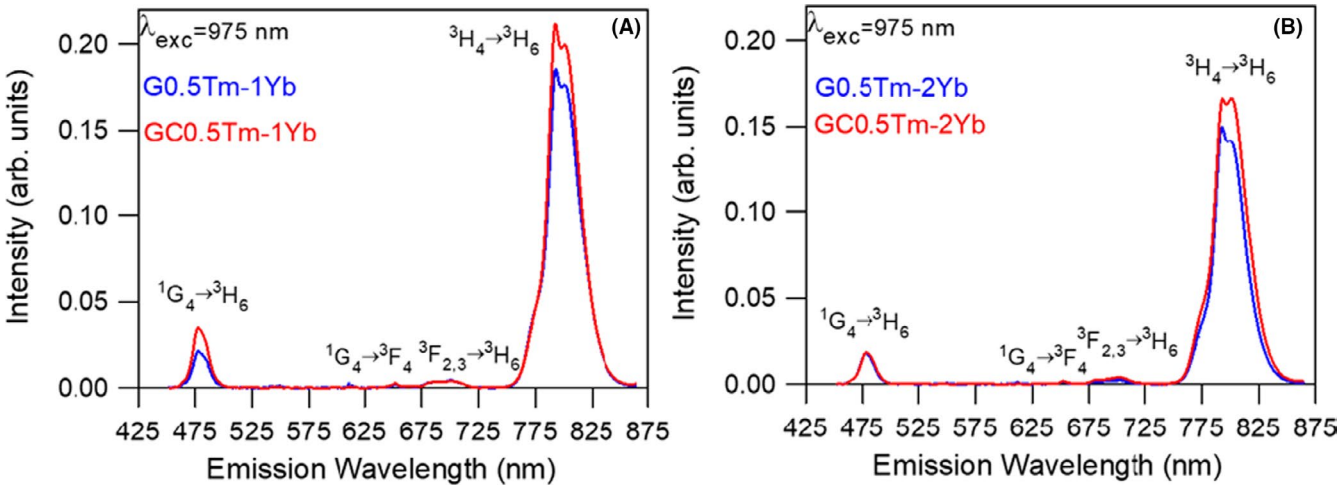

FIGURE 8 Room temperature UC emission spectra obtained under 975 nm excitation for glass (blue line) and GC (red line) samples codoped with 1 (A) and 2 (B) Yb^{3+}

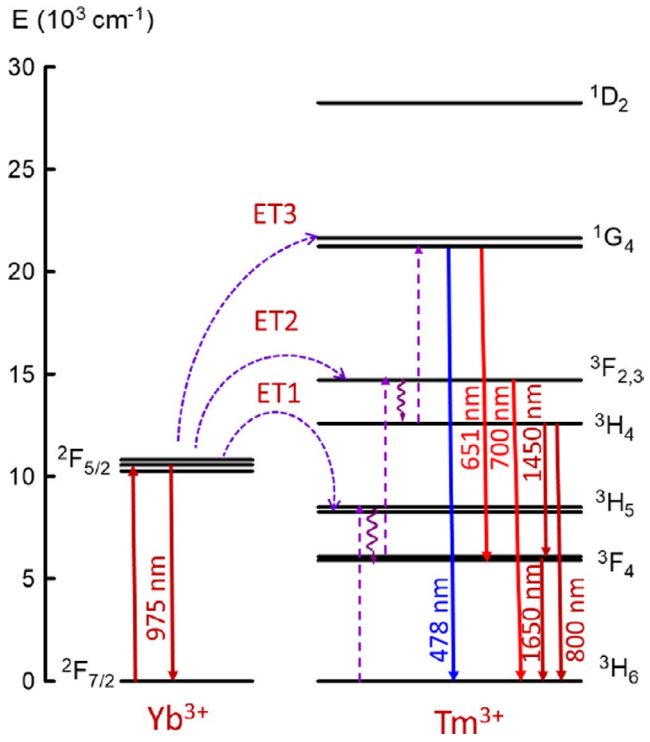

FIGURE 9 Energy level diagram of Yb^{3+} and Tm^{3+} ions together with the different energy transfer processes (ET) responsible for the upconverted emissions after excitation at 975 nm (Yb^{3+})

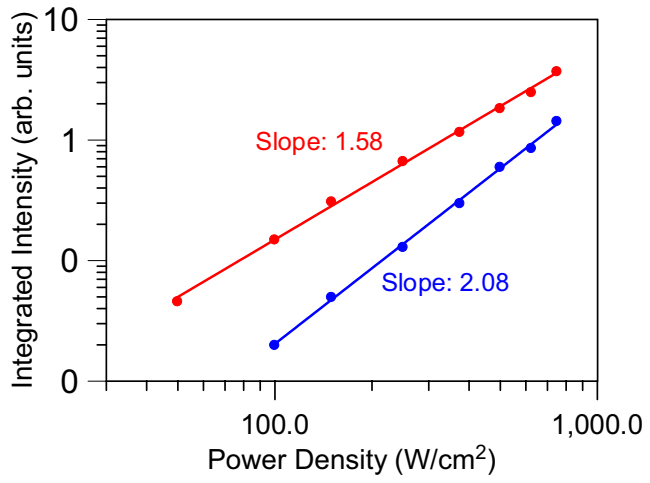

FIGURE 10 Logarithmic plot of the pump power dependence of the blue ($^1G_4 \rightarrow {}^3H_6$) and NIR ($^3H_4 \rightarrow {}^3H_6$) integrated emission intensities for the GC sample codoped with $0.5Tm^{3+}$-$1Yb^{3+}$

transfer process involving Yb^{3+} and Tm^{3+} ions can occur through the mechanism $^2F_{5/2} \rightarrow {}^2F_{7/2}$ (Yb^{3+}):$^3F_4 \rightarrow {}^3F_{2,3}$ (Tm^{3+}) (ET2). Subsequent multiphonon relaxation from level $^3F_{2,3}$ populates the $^3H_4$ state and a third energy transfer upconversion process, $^2F_{5/2} \rightarrow {}^2F_{7/2}$ (Yb^{3+}):$^3H_4 \rightarrow {}^1G_4$ (Tm^{3+}) (ET3) populates the $^1G_4$ state.[46]

To obtain information about the processes involved in the UC emission after 975 nm excitation, the UC emission spectra have been obtained at different pump power densities. The dependence of the UC emission on the pump power density is related to the number of photons (n) involved in the process and gives information about the UC mechanisms according to the relation

$$I_{em} \propto (P_{pump})^n. \quad (2)$$

Figure 10 shows the logarithmic plot of the UC blue and NIR ($^3H_4 \rightarrow {}^3H_6$) emission intensities of the co-doped GC sample with $0.5TmF_3$–$1YbF_3$ (in mol%) as a function of the pump power laser density. As can be seen for the blue emission, the slope is 2.08 which indicates that two photons are required to excite the electrons to the $^1G_4$ state. The slope in the case of the $^3H_4 \rightarrow {}^3H_6$ transition is 1.58. However, it is clear from the energy level diagram of Tm^{3+} ions (Figure 9) that two photons are needed to populate this level and three photons are needed to populate the $^1G_4$ level. UC to the $^3H_4$ level occurs via two successive energy transfers from Yb^{3+} ions in the $^2F_{5/2}$ excited state. An excited Yb^{3+} ion in the $^2F_{5/2}$ state transfers its energy nonresonantly to a Tm^{3+} ion in the ground state $^3H_6$, exciting it to the $^3H_5$ state from where the $^3F_4$ level is populated (ET1 in Figure 9). A second Yb^{3+} ion transfers its energy to the Tm^{3+} ion promoting it from the $^3F_4$ to the $^3F_{2,3}$ excited state (ET2 in Figure 9) and then decays nonradiatively to the$^3H_4$ level. A third energy transfer step from an excited Yb^{3+} ion can excite the Tm^{3+} ions to the $^1G_4$ level (ET3 in Figure 9). The observed slopes in Figure 10 indicate the presence of a saturation effect which reduces the experimental power dependence. The obtained power dependences represent the lower limit of the number of photons involved in the UC mechanisms.[50,51]

This behavior, previously observed in other systems, has been attributed to the competition between the decay rate of the intermediate states and the UC rates. When UC dominates over linear decay for the depletion of the intermediate excited states, the slope of the luminescence from the upper state n is almost linear.[52]

No UC emissions were observed in the single doped samples excited at 791 and 975 nm. However, UC emission of Tm^{3+} ions is also observed in the codoped glass and glass-ceramics samples with 1 and 2 mol% Yb^{3+} under 791 nm excitation (see Figure 11). This is probably due to the reduction of the interionic distances between the Tm^{3+} ions in the NCs favored by the presence of Yb^{3+} ions, increasing the probability of the Tm^{3+}-Tm^{3+} energy transfer. The UC mechanism of Tm^{3+}-Yb^{3+} codoped samples is as follows. After

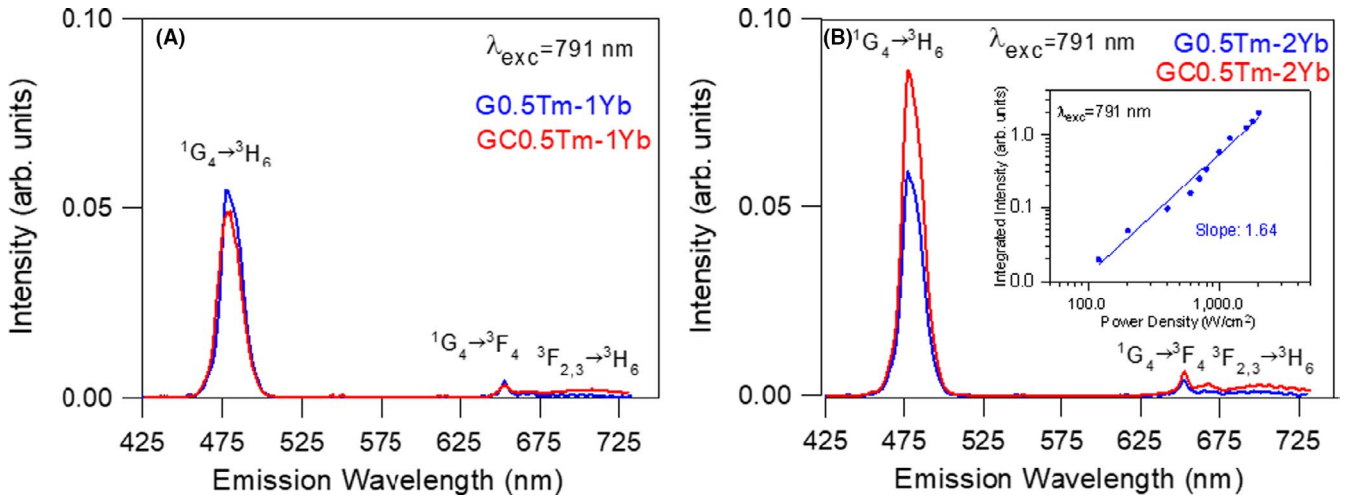

FIGURE 11 Room temperature upconversion emission spectra obtained under 791 nm excitation for the glass (blue line) and GC (red line) samples codoped with (A) 1 mol% Yb^{3+} and (B) 2 mol% Yb^{3+}. The inset in Figure 11B shows the pump power dependence of the blue UC emission

excitation of the ground state absorption at 791 nm, a photon with this energy populates the $^3H_4$ level and then the energy is transferred from Tm^{3+} to Yb^{3+} ions. This transfer is non-resonant with an energy mismatch of about 1800 cm^{-1}. The Yb^{3+} ions excited to the $^2F_{5/2}$ state transfer the energy to Tm^{3+} ions previously excited in the $^3H_4$ level which results in blue and red emissions from levels $^1G_4$ and $^3F_{2,3}$.[53] In order to analyze the upconversion mechanism which populates the $^1G_4$ level, the dependence of the blue integrated emission intensity on the pump power density has been analyzed for the GC sample co-doped with 2 mol% Yb^{3+}. The inset in Figure 11B shows the logarithmic plot of the blue ($^1G_4 \rightarrow {}^3H_6$) emission as a function of the pump power density for 791 nm excitation. The dependence is nearly quadratic with a slope of 1.64 which indicates a two-photon UC process in contrast with the result under 975 nm excitation in which the blue emission is the result of a three photon UC process. Since the probability of a two-photon mechanism is higher than that of a three-photon mechanism, the UC blue emission intensity observed for the codoped samples under 791 nm excitation is higher than under 975 nm excitation.

4 | CONCLUSIONS

Oxyfluoride GCs with a cubic solution of the type $Na_xLu_{2x-1}F_{7x-3}$ NCs have been successfully obtained by the melting quenching method and subsequent crystallization process using an optimized heat treatment at 600°C during 20h. The treatment allows precipitation of $NaLuF_4$ NCs with a mean size in the range of 9–30 nm, as confirmed by XRD and HRTEM. Shift to lower angles of XRD maxima with respect to the undoped-based GCs indicate the incorporation of the Tm^{3+} and Yb^{3+} ions in the NCs, also confirmed by STEM-EDX analysis. This is also demonstrated by the luminescence results. Energy transfer between Yb^{3+} and Tm^{3+} ions is confirmed by the NIR and UC conversion emissions after Yb^{3+} excitation at 975. NIR Yb^{3+} ($^2F_{5/2} \rightarrow {}^2F_{7/2}$) emission around 1000 nm is also observed after Tm^{3+} excitation at 791 nm due to a non-resonant phonon-assisted energy transfer (PAET) between both ions. Visible UC emissions are only observed in Tm^{3+}-Yb^{3+} codoped samples, thus confirming the effective energy transfer between Yb^{3+} and Tm^{3+} ions. The addition of Yb^{3+} also favours the UC emission of Tm^{3+} after excitation in codoped samples compared to the single Tm^{3+} doped ones, where no UC emission is observed. These effects are more pronounced in the GCs samples due to the reduction of the interionic distances after the incorporation of the RE ion in the NCs. Codoped samples can be thus used to tune the UC emission from NIR to blue by the selectivity of the excitation.

ACKNOWLEDGEMENTS

This work was supported by MINECO under Projects MAT2017-87035-C2-1-P/-2-P (AEI/FEDER, UE), Basque Country Government PIBA2018-24 and Basque Country University GIU17/014. This article is part of the dissemination activities of project FunGlass. This project has received funding from the European Union´s Horizon 2020 research and innovation programme under grant agreement No 739566. This article was also created in the frame of the project Centre for Functional and Surface Functionalized Glass (CEGLASS), ITMS code is 313011R453, operational program Research and innovation, co-funded from

European Regional Development Fund. This research work has been supported by the Research Agency of the Ministry of Education, Science, Research and Sport of the Slovak Republic, by the project: Advancement and support of R&D for "Centre for diagnostics and quality testing of materials" in the domains of the RIS3 SK specialization, Acronym: CEDITEK II., ITMS2014+ code 313011W442.

ORCID

Jose J. Velázquez https://orcid.org/0000-0001-7672-0539
Rolindes Balda https://orcid.org/0000-0001-6882-3167
Giulio Gorni https://orcid.org/0000-0001-8227-9022
Alicia Durán https://orcid.org/0000-0002-0067-1934
Dušan Galusek https://orcid.org/0000-0001-5995-8780
Maria J. Pascual https://orcid.org/0000-0002-6833-9663

REFERENCES

1. Blasse G, Luminescent GBC. Blasse and Grabmaier - 1994.pdf. Springer Series on Fluorescence, Vol. 7. 1994.
2. Desurvire E, Zervas MN. Erbium-doped fiber amplifiers: principles and applications. Phys Today. 1995;48(2):56–8.
3. Downing E, Hesselink L, Ralston J, Macfarlane R. A three-color, solid-state, three-dimensional display. Science. 1996;273(5279):1185–9.
4. Wang F, Han YU, Lim CS, Lu Y, Wang J, Xu J, et al. Simultaneous phase and size control of upconversion nanocrystals through lanthanide doping. Nature. 2010;463(7284):1061–5.
5. Huang X, Han S, Huang W, Liu X. Enhancing solar cell efficiency: the search for luminescent materials as spectral converters. Chem Soc Rev. 2013;42(1):173–201.
6. Krishnaiah KV, Ledemi Y, Genevois C, Veron E, Sauvage X, Morency S, et al. Ytterbium-doped oxyfluoride nano-glass-ceramic fibers for laser cooling. Opt Mater Express. 2017;7(6):1980.
7. Fedorov PP, Luginina AA, Popov AI. Transparent oxyfluoride glass ceramics. J Fluor Chem. 2015;172:22–50.
8. de Pablos-Martín A, Durán A, Pascual MJ. Nanocrystallisation in oxyfluoride systems: mechanisms of crystallisation and photonic properties. Int Mater Rev. 2012;57(3):165–86.
9. Shepilov MP, Dymshits OS, Zhilin AA. Light scattering in glass-ceramics: revision of the concept. J Opt Soc Am B. 2018;35(7):1717.
10. de Pablos-Martín A, Hémono N, Mather GC, Bhattacharyya S, Höche T, Bornhöft H, et al. Crystallization kinetics of LaF_3 nanocrystals in an oxyfluoride glass. J Am Ceram Soc. 2011;94(8):2420–8.
11. Ye S, Zhu B, Luo J, Chen J, Lakshminarayana G, Qiu J. Enhanced cooperative quantum cutting in Tm^{3+}–Yb^{3+} codoped glass ceramics containing LaF_3 nanocrystals. Opt Express. 2008;16(12):8989.
12. Chen D, Wang Y, Yu Y, Huang P. Intense ultraviolet upconversion luminescence from Tm^{3+}/Yb^{3+}:β-YF3 nanocrystals embedded glass ceramic. Appl Phys Lett. 2007;91(5):51920.
13. Cabral AA, Balda R, Fernández J, Gorni G, Velázquez JJ, Pascual L, et al. Phase evolution of $KLaF_4$ nanocrystals and their effects on the photoluminescence of Nd^{3+} doped transparent oxyfluoride glass-ceramics. CrystEngComm. 2018;20(38):5760–71.
14. Velázquez JJ, Balda R, Fernández J, Gorni G, Pascual L, Chen G, et al. Transparent oxyfluoride glass-ceramics with $NaGdF_4$ nanocrystals doped with Pr^{3+} and Pr^{3+}–Yb^{3+}. J Lumin. 2018;193:61–9.
15. de Pablos-Martín A, Mather GC, Muñoz F, Bhattacharyya S, Höche TH, Jinschek JR, et al. Design of oxy-fluoride glass-ceramics containing $NaLaF_4$ nano-crystals. J Non Cryst Solids. 2010;356(52–54):3071–9.
16. de Pablos-Martín A, Méndez-Ramos J, del-Castillo J, Durán A, Rodríguez VD, Pascual MJ. Crystallization and up-conversion luminescence properties of Er^{3+}/Yb^{3+}-doped $NaYF_4$-based nano-glass-ceramics. J Eur Ceram Soc. 2015;35(6):1831–40.
17. Liu Q, Sun Y, Yang T, Feng W, Li C, Li F. Sub-10 nm hexagonal lanthanide-doped $NaLuF_4$ upconversion nanocrystals for sensitive bioimaging in vivo. J Am Chem Soc. 2011;133(43):17122–5.
18. Wei Y, Liu X, Chi X, Wei R, Guo H. Intense upconversion in novel transparent $NaLuF_4$:Tb^{3+}, Yb^{3+} glass–ceramics. J Alloys Compd. 2013;578:385–8.
19. Ouyang J, Yin D, Cao X, Wang C, Song K, Liu B, et al. Synthesis of $NaLuF_4$ -based nanocrystals and large enhancement of upconversion luminescence of $NaLuF^4$:Gd, Yb, Er by coating an active shell for bioimaging. Dalt Trans. 2014;43(37):14001–8.
20. Wan Z, Chen D, Zhou Y, Huang P, Zhong J, Ding M, et al. Eu^{3+} and Er^{3+} doped $NaLu_1YbF_4$ (x= 0 ~ 1) solid-solution self-crystallization nano-glass-ceramics: microstructure and optical spectroscopy. J Eur Ceram Soc. 2015;35(13):3673–9.
21. Shmyt'ko IM, Strukova GK. Fine sructure of $Na_5Lu_9F_{32}$ nanocrystallites formed at the initial stages of crystallization. Phys Solid State. 2009;51(9):1907–11.
22. Chen D, Zhou Y, Wan Z, Huang P, Yu H, Lu H, et al. Enhanced upconversion luminescence in phase-separation-controlled crystallization glass ceramics containing Yb/Er(Tm): $NaLuF_4$ nanocrystals. J Eur Ceram Soc. 2015;35(7):2129–37.
23. Kück S, Sokólska I, Henke M, Scheffler T, Osiac E. Emission and excitation characteristics and internal quantum efficiencies of vacuum-ultraviolet excited Pr^{3+}-doped fluoride compounds. Phys Rev B. 2005;71(16):165112.
24. Aleshire CE, Yu CX, Reed PA, Fan TY. Efficient cryogenic near-infrared Tm:YLF laser. Opt Express. 2017;25(12):13408.
25. Braud A, Girard S, Doualan JL, Thuau M, Moncorgé R, Tkachuk AM. Energy-transfer processes in Yb:Tm-doped KY_3F_{10}, $LiYF_4$, and BaY_2F_8 single crystals for laser operation at 1.5 and 2.3 μm. Phys Rev B. 2000;61(8):5280–92.
26. Heine F, Ostroumov V, Heumann E, Jensen T, Huber G, Chai BHT. CW Yb,Tm:$LiYF_4$ upconversion laser at 650 nm, 800 nm, and 1500 nm. In: Chai B, Payne S, editors. Advanced solid state lasers. OSA Proceedings Series, Vol. 24. Washington, D.C.: Optical Society of America; 1995. p. VL4.
27. Méndez-Ramos J, Velázquez JJ, Yanes AC, Del-Castillo J, Rodriguez VD. Up-conversion in nanostructured Yb^{3+}-Tm^{3+} co-doped sol-gel derived SiO_2-LaF_3 transparent glass-ceramics. Phys Status Solidi Appl Mater Sci. 2008;205(2):330–4.
28. Velázquez JJ, Balda R, Fernández J, Gorni G, Mather GC, Pascual L, et al. Transparent glass-ceramics of sodium lutetium fluoride co-doped with erbium and ytterbium. J Non Cryst Solids. 2018;501:136–44.
29. Gorni G, Velázquez JJ, Kochanowicz M, Dorosz D, Balda R, Fernández J, et al. Tunable upconversion emission in $NaLuF_4$

–glass-ceramic fibers doped with Er^{3+} and Yb^{3+}. RSC Adv. 2019;9(54):31699–707.
30. Pascual MJ, Garrido C, Durán A, Miguel A, Pascual L, de Pablos-Martín A, et al. Optical properties of transparent glass-ceramics containing Er^{3+} -doped sodium lutetium fluoride nanocrystals. Int J Appl Glas Sci. 2016;7(1):27–40.
31. Cullity BD, Weymouth JW. Elements of X-ray Diffraction. Am J Phys. 1957;25(6):394–5.
32. Środa M, Wacławska I, Stoch L, Reben M. DTA/DSC study of nanocrystallization in oxyfluoride glasses. J Therm Anal Calorim. 2004;77(1):193–200.
33. Gorni G, Velázquez JJ, Mather GC, Durán A, Chen G, Sundararajan M, et al. Selective excitation in transparent oxyfluoride glass-ceramics doped with Nd^{3+}. J Eur Ceram Soc. 2017;37(4):1695–706.
34. Reben M, Środa M. Influence of fluorine on thermal properties of lead oxyfluoride glass. J Therm Anal Calorim. 2013;113(1):77–81.
35. Gorni G, Velázquez JJ, Kochanowicz M, Dorosz D, Balda RB, Fernandez J, et al. Tunable upconversion emission in $NaLuF_4$-glass-ceramic fibers doped with Er^{3+} and Yb^{3+}. Proc. SPIE: Fiber Lasers and Glass Photonics: Materials through Applications II, 113570B. 2020;11357:54–9.
36. Katayama Y, Tanabe S. Near infrared downconversion in Pr^{3+}–Yb^{3+} codoped oxyfluoride glass ceramics. Opt Mater (Amst). 2010;33(2):176–9.
37. Velázquez JJ, Yanes AC, del Castillo J, Méndez-Ramos J, Rodríguez VD. Optical properties of Ho^{3+}-Yb^{3+} co-doped nanostructured SiO_2 -LaF_3 glass-ceramics prepared by sol-gel method. Phys Status Solidi. 2007;204(6):1762–8.
38. Yu Y, Chen D, Cheng Y, Wang Y, Hu Z, Bao F. Investigation on crystallization and influence of Nd^{3+} doping of transparent oxyfluoride glass-ceramics. J Eur Ceram Soc. 2006;26(13):2761–7.
39. Gorni G, Cosci A, Pelli S, Pascual L, Durán A, Pascual MJ. Transparent oxyfluoride nano-glass ceramics doped with Pr^{3+} and Pr^{3+}–Yb^{3+} for NIR emission. Front Mater. 2017;3:58.
40. Velázquez JJ, Gorni G, Balda R, Fernández J, Pascual L, Durán A, et al. Non-linear optical properties of Er^{3+}–Yb^{3+}-doped $NaGdF_4$ nanostructured glass-ceramics. Nanomaterials. 2020;10(7):1425.
41. Liu F, Ma E, Chen D, Yu Y, Wang Y. Tunable red-green upconversion luminescence in novel transparent glass ceramics containing Er: $NaYF_4$ nanocrystals. J Phys Chem B. 2006;110(42):20843–6.
42. Balda R, Gorni G, Velázquez JJ, Pascual MJ, Durán A, Fernández J. Chapter 16 performance of Nd^{3+} as structural probe of rare-earth distribution in transparent nanostructured glass-ceramics. In: Di Bartolo D, Silvestri L, Cesaria M, Collins J, editors. Quantum Nano-Photonics. NATO Science for Peace and Security Series B: Physics and Biophysics. Dordrecht, The Netherlands: Springer; 2018. p. 297–313.
43. Tick P, Borrelli N, Reaney I. The relationship between structure and transparency in glass-ceramic materials. Opt Mater (Amst). 2000;15(1):81–91.
44. Beall GH, Duke DA. Transparent glass-ceramics. J Mater Sci. 1969;4(4):340–52.
45. Brenier A, Pedrini C, Moine B, Adam JL, Pledel C. Fluorescence mechanisms in Tm^{3+} singly doped and Tm^{3+}, Ho^{3+} doubly doped indium-based fluoride glasses. Phys Rev B. 1990;41(8):5364–71.
46. Albalawi A, Varas S, Chiasera A, Gebavi H, Albalawi W, Blanc W, et al. Determination of reverse cross-relaxation process constant in Tm-doped glass by 3H4 fluorescence decay tail fitting. Opt Mater Express. 2017;7(10):3760.
47. Falconi MC, Laneve D, Portosi V, Taccheo S, Prudenzano F. Design of a multi-wavelength fiber laser based on Tm:Er:Yb: Ho co-doped germanate glass. J Light Technol. 2020;38(8):2406–13.
48. Lukowiak A, Stefanski M, Ferrari M, Strek W. Nanocrystalline lanthanide tetraphosphates: energy transfer processes in samples co-doped with Pr^{3+}/Yb^{3+} and Tm^{3+}/Yb^{3+}. Opt Mater (Amst). 2017;74:159–65.
49. Quintanilla M, Núñez NO, Cantelar E, Ocaña M, Cussó F. Energy transfer efficiency in YF_3 nanocrystals: Quantifying the Yb^{3+} to Tm^{3+} infrared dynamics. J Appl Phys. 2013;113(17):174308.
50. Pollnau M, Gamelin DR, Lüthi SR, Güdel HU, Hehlen MP. Power dependence of upconversion luminescence in lanthanide and transition-metal-ion systems. Phys Rev B. 2000;61(5):3337–46.
51. Halubek-Gluchowska K, Szymański D, Tran TNL, Ferrari M, Lukowiak A. Upconversion luminescence of silica-calcia nanoparticles co-doped with Tm^{3+} and Yb^{3+} ions. Materials (Basel). 2021;14(4):937.
52. Suyver JF, Aebischer A, García-Revilla S, Gerner P, Güdel HU. Anomalous power dependence of sensitized upconversion luminescence. Phys Rev B. 2005;71(12):125123.
53. Lahoz F, Martín IR, Méndez-Ramos J, Núñez P. Dopant distribution in a Tm^{3+}–Yb^{3+} codoped silica based glass ceramic: an infrared-laser induced upconversion study. J Chem Phys. 2004;120(13):6180–90.

How to cite this article: Velázquez JJ, Balda R, Fernández J, Gorni G, Sedano M, Durán A, et al. Structural and optical properties in Tm^{3+}/Tm^{3+}–Yb^{3+} doped $NaLuF_4$ glass-ceramics. Int J Appl Glass Sci. 2021;00:1–12. https://doi.org/10.1111/ijag.16322